Chinese Chemical Letters 33 (2022) 939–942

Contents lists available at ScienceDirect

Chinese Chemical Letters

journal homepage: www.elsevier.com/locate/cclet

The Z-scheme g-C_3N_4/3DOM-WO_3 photocatalysts with enhanced activity for CO_2 photoreduction into CO

Zhiling Tang[a,b,1], Chujun Wang[a,1], Wenjie He[a,b], Yuechang Wei[a,b,*], Zhen Zhao[a], Jian Liu[a]

[a] State Key Laboratory of Heavy Oil Processing, China University of Petroleum, Beijing 102249, China
[b] Key Laboratory of Optical Detection Technology for Oil and Gas, China University of Petroleum, Beijing 102249, China

ARTICLE INFO

Article history:
Received 21 April 2021
Revised 16 June 2021
Accepted 6 July 2021
Available online 13 July 2021

Keywords:
3DOM-WO_3
g-C_3N_4
Z-scheme heterojunction
CO_2 conversion
Photocatalysis

ABSTRACT

The catalytic performance of light-derived CO_2 reduction with H_2O is strongly dependent on the separation efficiency of photogenerated carriers. Herein, the direct Z-scheme catalysts (g-C_3N_4/3DOM-WO_3) of graphitic carbon nitride (g-C_3N_4) nanosheets decorated three-dimensional ordered macroporous WO_3 (3DOM-WO_3) were successfully fabricated by using the *in-situ* colloidal crystal template method. The slow light effect of 3DOM-WO_3 photonic crystals expands the absorption of visible light and improves the utilization of light energy. The Z-scheme structure of g-C_3N_4/3DOM-WO_3 catalysts is able to upgrade the separation efficiency of photogenerated electron-hole pairs. The g-C_3N_4/3DOM-WO_3 photocatalyst, whose formation rate of CO product is 48.7 μmol g^{-1} h^{-1}, exhibits the excellent catalytic activity for CO_2 reduction. The transfer pathway of stimulated electrons over the g-C_3N_4/3DOM-WO_3 photocatalyst is proposed and discussed. The present approach provides unique insights into the rational development of high-performance photochemical systems for efficient CO_2 reduction into valuable carbon-containing chemicals and energy fuels.

For controlling of the damage by CO_2 [1-5], photocatalytic CO_2 conversion technology is employed [6,7]. The initial research [8] has studied solar light driving artificial photosynthesis widely [9,10]. Especially, the heterojunction materials have caught the eyes [11,12].

Layer graphite carbon nitride (g-C_3N_4) possesses a certain photocatalytic activity [13-17], which the narrow band gap (2.7 eV) responds to visible light [18], but suffer from the rapid recombination of photoinduced e^-/h^+ pairs. Fortunately, the formation of g-C_3N_4/metal oxides heterojunction contributes to the separation efficiency of carriers [19-25]. Among a large number of metal oxides that have been widely studied for photocatalytic conversion of CO_2, tungsten oxide (WO_3) is considered to be one of the promising materials due to its high oxidation potential and special catalytic properties [26]. The optical band gap of WO_3 is narrow (2.7 eV), and the holes generated on the valence band of WO_3 have strong oxidation ability. However, it is still a challenge to further modify WO_3 for improving the photocatalytic activity due to the low absorption and utilization efficiency of solar energy.

Three-dimensional ordered macroporous (3DOM) materials, billed as inverse opals, encompasses photonic crystals with regular and uniform porous structure. Photonic crystals have periodic modulations of the refractive index on the length scale of light wavelength [27]. The aperture of macropore is matched with a certain wavelength of light wave. So the light can propagate in it and be prevented from passing through Bragg diffraction, which is beneficial for the generation of energy band gap [28]. It has been found that 3DOM structure has the slow photon effect, which increases the length of light reaction path and enhances the light absorption efficiency of material during CO_2 photoreduction [29-33]. However, there are relatively few studies devoted to the design of WO_3 as 3DOM structure. Therefore, the Z-scheme photocatalyst with g-C_3N_4/3DOM-WO_3 heterojunction is fabricated for improving photocatalytic activity. The photogenerated media belonging to g-C_3N_4 and WO_3 will migrate because the different positions of valence band (VB) and conduction band (CB), which achieves effective separation of photogenerated electrons and holes. Consequently, the fabrication of Z-scheme heterojunction photocatalyst refers to a spectacular strategy to bring high-performance catalytic activity to CO_2 photo reduction.

Herein, the direct Z-scheme photocatalysts of g-C_3N_4 nanosheets decorated 3DOM-WO_3 (g-C_3N_4/3DOM-WO_3, abbreviated to 3DOM-CNW) were successfully fabricated by *in-situ*

* Corresponding author.
E-mail address: weiyc@cup.edu.cn (Y. Wei).
[1] These authors contributed equally to this work.

https://doi.org/10.1016/j.cclet.2021.07.020
1001-8417/

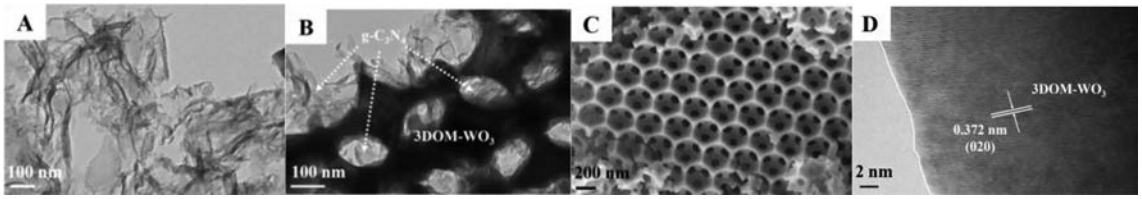

Fig. 1. TEM and HRTEM images of g-C_3N_4 (A), 3DOM-CNW-4 (B), 3DOM-WO_3 (D) photocatalysts, and SEM image of 3DOM-WO_3 (C) photocatalyst.

colloidal crystal template method. The Z-scheme heterojunction structure of 3DOM-CNW catalysts enhances the separation efficiency of photogenerated electron-hole pairs, which leads to the improvement of the catalytic activity for CO_2 photoreduction. The separation mechanism of photogenerated carriers in composite photocatalyst was proposed.

The 3DOM-WO_3 material was synthesized in virtue of colloidal crystal template (CCT) method, and 3DOM-CNW catalysts were fabricated by *in-situ* growing of g-C_3N_4 film on the pore wall of 3DOM-WO_3 as description in Supporting Information. During the *in-situ* synthesis processes of 3DOM-CNW catalysts, the mass ratios of g-C_3N_4 precursor (urea) and 3DOM-WO_3 are 2:1 and 4:1, which are denoted as 3DOM-CNW-2 and 3DOM-CNW-4, respectively. As shown in Fig. 1A, the two-dimensional silk-like ultrathin film of pure g-C_3N_4 can be observed, and their uniform ultrathin layers are potential to increase the specific surface area. The *d*-spacings of 0.372 nm (Fig. 1D) could be assigned to (020) crystal planes of WO_3 support. Figs. 1B and C clearly show the ordered and consistent macroporous structure. After introduction of g-C_3N_4 nanosheets, the macroporous structures of 3DOM-WO_3 and 3DOM-CNW-4 catalysts were perfect, indicating that the prepared procedures of 3DOM-CNW photocatalysts by *in-situ* growth method cannot destroy the 3DOM structure of WO_3 support.

To research the phase structure of 3DOM-WO_3 and g-C_3N_4 in 3DOM-CNW photocatalysts, the XRD patterns of g-C_3N_4, WO_3, 3DOM-CNW-2 and 3DOM-CNW-4 catalysts are shown in Fig. S1 (Supporting information). For the pure g-C_3N_4, the diffraction peak (2θ) of pure g-C_3N_4 nanocrystals at 27.1° can be indexed to the (002) crystal facets of g-C_3N_4 (JCPDS No. 87-1526), which is ascribed to the long-range interfacial stacking of the aromatic system. Another characteristic peak located at 13.0° is attributed to the in-plane structure stacking pattern [34]. According to the results of XRD patterns, the characteristic peaks of 3DOM-WO_3 support in the catalysts can be clearly observed, which are highly consistent with the standard monoclinic phase of WO_3 (JCPDS No. 20-1324). After introduction of a small volume of g-C_3N_4, the diffraction pattern of 3DOM-CNW-2 exhibits no obvious peaks indicative of crystalline phases. With increasing of g-C_3N_4 contents, the characteristic peak corresponding to (002) crystal plane of g-C_3N_4 can be found, and its diffraction peak intensity increases, while the intensity of diffraction peaks corresponding to 3DOM-WO_3 decreases. It suggests that the surface of 3DOM-WO_3 support is covered by g-C_3N_4 gradually. It is also noted that the diffraction peak of g-C_3N_4 (002) crystal plane shifts from 27.1° to 27.8°, indicating that the coupling between g-C_3N_4 and 3DOM-WO_3 may be related to the g-C_3N_4 (002) facets, which is ascribed to the interaction between 3DOM-WO_3 and g-C_3N_4 in the composite photocatalysts [35]. In addition, the shortened interlayer spacing of g-C_3N_4 results from the shift of the (002) diffraction peak, which is conducive to carrier transmission.

The functional groups and chemical bonds of photocatalysts were investigated by FT-IR (Fig. S2 in Supporting information). The absorption peaks of as-synthesized catalysts at 1248, 1325 and 1412 cm^{-1} are assigned to the stretching vibrations occurring to

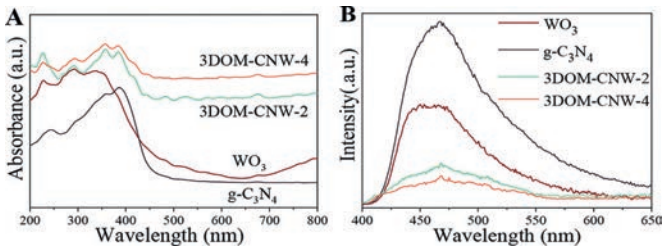

Fig. 2. UV-vis DRS (A) and PL spectra (B) of g-C_3N_4, WO_3, 3DOM-CNW-2 and 3DOM-CNW-4 catalysts.

the aromatic C–N bond, and the C–N stretching vibration peaks center at 1572 and 1639 cm^{-1}. For the g-C_3N_4, 3DOM-CNW-2 and 3DOM-CNW-4 catalysts, the characteristic peak at 808 cm^{-1} is stemmed out of the out-of-plane ring vibration of triazine structure and attributed to the C–N heterocycle in the samples. In addition, the presence of a broad absorption peak at the wavenumber of 3137 cm^{-1} is assigned to absorption conducted by water and N–H vibration in amine group. FT-IR can further prove that the 3DOM-CNW catalysts are encompassing g-C_3N_4 and 3DOM-WO_3, which is consistent with the results of TEM and XRD.

Fig. 2A exhibits the UV-vis diffuse reflectance spectroscopy of 3DOM-WO_3, g-C_3N_4, 3DOM-CNW-2 and 3DOM-CNW-4 catalysts. Compared with 3DOM-WO_3 and g-C_3N_4, the light absorption efficiency of 3DOM-CNW catalysts increases significantly, and the absorption edge of 3DOM-CNW displays red shift. It results in the enhanced light absorption capacity featured by the 3DOM-CNW with the integration of the g-C_3N_4 and 3DOM-WO_3. Thus, 3DOM-CNW catalysts with enhanced visible-light absorption efficiency make up the hopeful applications in photocatalytic reduction of CO_2. The photoluminescence (PL) spectrum is employed to evaluate the separation efficiency of photogenerated carriers and result is exhibited in Fig. 2B. The PL spectra of pure g-C_3N_4 and 3DOM-CNW catalysts have similar shapes and emission peaks located at 460 nm. The high intensity PL peak of pure g-C_3N_4 is assigned to the prompt reorganization of its own photogenerated carriers. The lower luminescence intensity of 3DOM-CNW catalyst indicates that the recombination of photogenerated electron-hole pairs encounters severe obstacle resulting from the coupling of g-C_3N_4 and 3DOM-WO_3 catalysts. The 3DOM-CNW-4 catalyst displays the lowest intensity compared to other catalysts at the same test conditions, which shows the huge reduction of reorganization rate for photogenerated electron-hole pairs. It demonstrates that 3DOM-CNW catalyst greatly improves the separation efficiency harbored by photogenerated carriers and expands the response range of visible light.

The promoted carrier transfer property of catalysts was evaluated by electrochemical impedance spectroscopy (EIS) in Na_2SO_4 solution (0.1 mol/L) under the condition of bias voltage of −1.3 V *vs.* RHE, and the frequency range is 10,000 Hz to 0.1 Hz. The Nyquist plots of WO_3, 3DOM-CNW-2 and 3DOM-CNW-4 catalysts are shown in Fig. S3 in Supporting information (light intensity

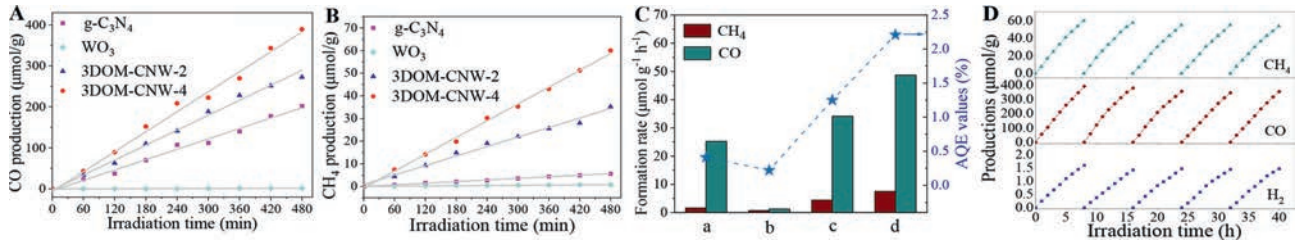

Fig. 3. CO (A) and CH_4 (B) products over g-C_3N_4, WO_3, 3DOM-CNW-2 and 3DOM-CNW-4 catalysts. (C) Product yields of CO and CH_4 and the AQE over the catalysts. (D) The stability of the formation rate of products (CH_4, CO and H_2) over the 3DOM-CNW-4 catalyst for five test cycles.

marks 80 mW/cm^2). The radius of semicircle in the spectrum is proportional to the charge transfer resistance (R_{ct}) of catalysts, which stands for the charge transfer capacity of catalysts and reactants. It is generally accepted that the lower the charge transfer resistance (R_{ct}), the faster the charge transfer process. 3DOM-CNW-4 catalyst has the smallest arc, indicating that photogenerated electron-hole pairs has effective separation in 3DOM-CNW-4 catalyst. On the basis of UV-vis DRS, PL and EIS obtained in the study, it can be confirmed that the 3DOM-CNW-4 catalyst has the best capability of visible-light capture as well as the separation efficiency of photogenerated carriers. The excited charges are rapidly transferred to the active surface of the 3DOM-CNW photocatalysts and interact with CO_2 to complete the reduction reaction.

To further investigate the chemical components and electronic sates of elements in the Z-scheme 3DOM-CNW catalysts, the X-ray photoelectron spectroscopy (XPS) spectra of W 4f regions for 3DOM-CNW catalysts was carried out as shown in Fig. S4. The existence of W(VI) in 3DOM-WO_3 catalyst is evidenced by the main peaks at 35.9 and 38.0 eV, which are assigned to the W $4f_{7/2}$ together with W $4f_{5/2}$ of W^{6+} species in WO_3 [36]. In contrast to 3DOM-WO_3 catalyst, the peaks of W element in 3DOM-CNW-4 catalyst are shifted to lower energy by 0.1-0.2 eV, revealing that the introduction of g-C_3N_4 can decrease the oxidation state of W in WO_3. It had been found that the binding energy of carbon element and nitrogen element has a positive shift [37]. Combined with the results of binding energy reduction of tungsten element, it indicates that the interaction between g-C_3N_4 and WO_3 causes the electron density to migrate from g-C_3N_4 to WO_3. After the generation of charge carriers, the binding effect of WO_3 on photoelectrons is weakened, the higher electron mobility in WO_3 directly injects the excited electron flow from its CB to the VB of g-C_3N_4.

Under the simulated irradiation of visible light ($\geq$ 420 nm), the photocatalytic performance of 3DOM-CNW photocatalysts for CO_2 reduction was evaluated in a closed gas-circulation system in the presence of water vapor. And the product was analyzed by gas chromatography. Fig. 3 and Table S1 (Supporting information) exhibit the catalytic performances of 3DOM-CNW catalysts for CO_2 photoreduction with H_2O. As revealed in Figs. 3A and B, the pure g-C_3N_4 nanosheets show excellent performance in converting CO_2 to CO, and the CO formation rate is 25.2 μmol g^{-1} h^{-1}, but the CH_4 product is undetected. During photocatalytic CO_2 reduction reaction, 3DOM-WO_3 catalyst has the low activity, which is attributed to the lower conduction band position of 3DOM-WO_3 catalyst. Compared with single-phase 3DOM-WO_3 and g-C_3N_4, the 3DOM-CNW binary catalyst has better photocatalytic performance for CO_2 reduction, demonstrating that the integration of 3DOM-WO_3 and g-C_3N_4 constitutes the direct Z-scheme heterojunction. The spatial separation of photogenerated electron-hole pairs is reliably formed. The 3DOM-CNW-4 catalyst exhibits the optimal formation rate of CO (48.7 μmol g^{-1} h^{-1}), and its formation rate of CH_4 is 7.5 μmol g^{-1} h^{-1}. Moreover, we further confirmed the formation rate of O_2 over the as-prepared catalysts. Among all the catalysts, 3DOM-CNW-4 catalyst shows the highest formation rate of O_2 (44.5 μmol g^{-1} h^{-1}), which is higher than the stoichiometric rate according to the calculation of other production (39.45 μmol g^{-1} h^{-1}). It may be attributed to the formation of other undetected hydrocarbons [38]. Therefore, it is concluded that 3DOM-CNW photocatalysts have the capability of upgrading the activity for CO_2 photo reduction because of its high photogenerated carrier separation and visible light capture efficiency.

The utilization efficiency of solar energy presents great significance for the photocatalytic reduction of CO_2 with H_2O as a reducing agent. The apparent quantum efficiency (AQE) is considered as a significant parameter in terms of the conversion of light energy and chemical energy. In Table S1, 3DOM-CNW-4 photocatalyst shows the highest AQE value (2.21), which is 110-fold of that of 3DOM-WO_3 photocatalyst (0.02). It further confirms that the *in-situ* growing g-C_3N_4 in three-dimensional ordered macropores is an effective strategy for improving the application efficiency of solar energy. To investigate the stability of the formation rate of products (CH_4, CO and H_2) over 3DOM-CNW-4 photocatalyst, five activity test cycles were carried out under the exactly same conditions. As demonstrated in Fig. 3D, after the five test cycles, the formation rate of the products maintains the same high activity trend and exhibits no obvious decrease, indicating that the 3DOM-CNW photocatalysts have excellent cycle stability for CO_2 photoreduction.

According to the results of XPS, 3DOM-CNW photocatalysts have achieved the electron transmission path from 3DOM-WO_3 (CB) to g-C_3N_4 (VB) (Fig. 4A). On the basis of the above results, the mechanism of Z-scheme 3DOM-CNW photocatalysts for CO_2 reduction is proposed (Fig. 4A). In general, WO_3 has lower Fermi energy level and larger work function (6.23 eV), while g-C_3N_4 is a semiconductor with higher Fermi energy level and smaller work function (4.18 eV) (Fig. 4B). *In situ* growth of g-C_3N_4 film uniformly on the pore wall of 3DOM-WO_3 can promote the electrons transfer between g-C_3N_4 and 3DOM-WO_3 spontaneously until their Fermi levels are the same (Fig. 4C). Therefore, the internal electric field is obtained because of the opposite charges of 3DOM-WO_3 and g-C_3N_4. Derived out of the charge accumulation, the energy band edge of 3DOM-WO_3 is bent downward, while the energy band edge of g-C_3N_4 is bent upward resulting from the loss of electrons. Under light irradiation, the electrons are excited from VB to CB of both WO_3 and g-C_3N_4. The internal electric field, band edge bending and Coulomb interaction accelerate the recombination of some electrons (from CB of WO_3) and holes (from VB of g-C_3N_4). Hence, electrons with more negative potential provide powerful driving force oriented with the photocatalytic reduction of CO_2 to CH_4 and CO. In the half-reaction of water at the position of the VB of 3DOM-WO_3 with higher positive potential, the hydroxide radical is oxidized to generate O_2 and active hydrogen, which is an important active species that promotes carbon dioxide deoxygenation. Therefore, the oxygen generation reaction at the position of the VB plays an important role in the photocatalytic reduction

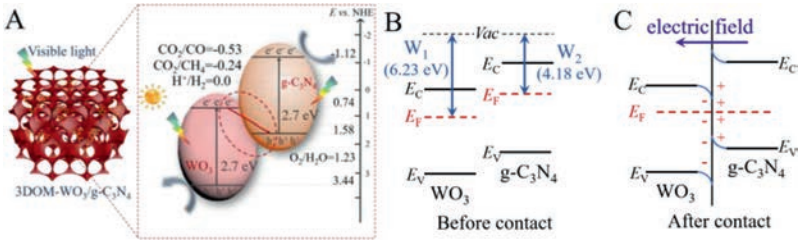

Fig. 4. (A) The mechanism of 3DOM-CNW photocatalyst for photocatalytic CO_2 reduction with H_2O. (B) This work functions of 3DOM-WO_3 and g-C_3N_4. (C) The formation of internal electric field and the variety of band edge at the interface of g-C_3N_4/3DOM-WO_3 after contact.

of CO_2. In addition, the ultrathin layers structure from g-C_3N_4 as well as the macroporous structure of 3DOM-WO_3 cleverly increase the contact area. The promoted interaction provides a straight path for electrons transfer from 3DOM-WO_3 to g-C_3N_4. The photogenerated holes in g-C_3N_4 are quenched by this rapid electron injection, and the reorganization of photogenerated electron-hole pairs is effectively inhibited. Simultaneously, the low fluorescence intensity of 3DOM-CNW-4 also strongly proves that there is charge separation on the interface where 3DOM-WO_3 and g-C_3N_4 (Fig. 2B) are coexisting. In other words, the 3DOM-CNW direct Z-scheme photocatalyst not only realizes the rapid separation of photogenerated carriers, but also retains a better redox potential. The charge carrier transfer process (Fig. 4A) and the formation of internal electric field (Fig. 4C) are two important factors for the excellent redox capability of the 3DOM-CNW heterojunction photocatalyst, which is very beneficial for the photocatalytic reduction of CO_2.

Herein, the photonic crystal 3DOM-WO_3 was prepared by the colloidal crystal template method, and 3DOM-CNW catalysts were fabricated by *in-situ* growing of g-C_3N_4 film on the pore wall of 3DOM-WO_3. The CB position of 3DOM-WO_3 is close to the VB position of g-C_3N_4, which provides new sight for the construction of the all-solid-state Z-scheme photocatalyst for visible-light driving photocatalytic CO_2 reduction with H_2O. 3DOM-CNW catalyst overcomes the shortcomings of the mismatch between the CB position of traditional semiconductor materials and the redox potential required for the reaction. By constructing the direct Z-scheme system, the higher redox potential can be retained, which can realize the directional conduction of electrons between the double semiconductor materials, thereby separating the reduction and oxidation reactions. 3DOM-CNW catalysts have high the harvest efficiency of visible-light and the separation efficiency of photogenerated electron-hole pairs. 3DOM-CNW catalysts are representing outstanding performance for photocatalytic CO_2 reduction, and the formation rates of CO and CH_4 products over 3DOM-CNW-4 catalysts are 48.7 and 7.5 $\mu mol\ g^{-1}\ h^{-1}$, respectively. The electron transfer mechanism was studied and verified. This research provides a new avenue for the construction of direct Z-scheme photocatalysts.

Declaration of competing interest

The authors declare that they have no known competing financial interests or personal relationships that could have appeared to influence the work reported in this paper.

Acknowledgments

This work was supported by the National Natural Science Foundation of China (No. 21972166), Beijing Natural Science Foundation (No. 2202045) and National Key Research and Development Program of China (No. 2019YFC1907600).

Supplementary materials

Supplementary material associated with this article can be found, in the online version, at doi:10.1016/j.cclet.2021.07.020.

References

[1] Y. Liu, T. Wang, X. Fang, et al., Chin. Chem. Lett. 31 (2020) 2712–2716.
[2] Y. Izumi, Coord. Chem. Rev. 257 (2013) 171–186.
[3] A.D. Tjandra, J. Huang, Chin. Chem. Lett. 29 (2018) 734–746.
[4] M. Marszewski, S. Cao, J. Yu, M. Jaroniec, Mater. Horiz. 2 (2015) 261–278.
[5] I.I. Alkhatib, C. Garlisi, M. Pagliaro, K. Al-Ali, G. Palmisano, Catal. Today. 340 (2020) 209–224.
[6] A. Dhakshinamoorthy, S. Navalon, A. Corma, H. Garcia, Energ. Environ. Sci. 5 (2012) 9217–9233.
[7] X. Chang, T. Wang, J. Gong, Energ. Environ. Sci. 9 (2016) 2177–2196.
[8] T. Inoue, A. Fujishima, S. Konishi, K. Honda, Nature 277 (1979) 637–638.
[9] F Wang, X Yu, M Ge, S Wu, Chem. Eng. J. 384 (2020) 123381.
[10] K. Zhang, G. Lu, Z. Xi, et al., Chin. Chem. Lett. 32 (2021) 2207–2211.
[11] Y. Wei, J. Jiao, Z. Zhao, et al., J. Mater. Chem. A 3 (2015) 11074–11085.
[12] W. He, X. Wu, Y. Li, et al., Chin. Chem. Lett. 31 (2020) 2774–2778.
[13] X. Wang, K. Maeda, A. Thomas, et al., Nature Mater 8 (2009) 76–80.
[14] J. Yan, H. Wu, H. Chen, et al., Appl. Catal. B 191 (2016) 130–137.
[15] F. Mu, B. Dai, W. Zhao, et al., Chin. Chem. Lett. 31 (2020) 1773–1781.
[16] C. Wang, X. Liu, W. He, et al., J. Catal. 389 (2020) 440–449.
[17] X. Zhao, Y. Fan, W. Zhang, et al., ACS Catal. 10 (2020) 6367–6376.
[18] Y. Li, M. Gu, X. Zhang, et al., Mater. Today 41 (2020) 270–303.
[19] X Pan, J Ji, N Zhang, M Xing, Chin. Chem. Lett. 31 (2020) 1462–1473.
[20] L. Zhou, J. Feng, B. Qiu, et al., Appl. Catal. B 267 (2020) 118396.
[21] X. Chen, Q. Chen, W. Jiang, Z. Wei, Y. Zhu, Appl. Catal. B 211 (2017) 106–113.
[22] X. Wang, G. Liu, Z. Chen, et al., Chem. Commun. 23 (2009) 3452–3454.
[23] C. Wang, Y. Zhao, H. Xu, et al., Appl. Catal. B 263 (2020) 118314.
[24] W. Pei, Y. Liu, J. Deng, et al., Appl. Catal. B 256 (2019) 117814.
[25] T. Takata, A. Tanaka, M. Hara, et al., Catal. Today. 44 (1998) 17–26.
[26] J. Kim, C.W. Lee, W. Choi, Environ. Sci. Technol. 44 (2010) 6849–6854.
[27] M. Wu, Y. Li, Z. Deng, B.-L. Su, ChemSusChem 4 (2011) 1481–1488.
[28] M. Zhou, J. Bao, Y. Xu, et al., ACS Nano 8 (2014) 7088–7098.
[29] K. Ji, J. Deng, H. Zang, et al., Appl. Catal. B 165 (2015) 285–295.
[30] J. Jiao, Y. Wei, Y. Zhao, et al., Appl. Catal. B 209 (2017) 228–239.
[31] X. Wu, C. Wang, Y. Wei, et al., J. Catal. 377 (2019) 309–321.
[32] T. Kamegawa, N. Suzuki, H. Yamashita, Energ. Environ. Sci. 4 (2011) 1411–1416.
[33] J. Liu, G. Liu, M. Li, et al., Energ. Environ. Sci. 3 (2010) 1503–1506.
[34] X. Li, B. Kang, F. Dong, et al., Nano Energy 81 (2021) 105671.
[35] L. Ye, J. Liu, Z. Jiang, T. Peng, L. Zan, Appl. Catal. B 142-143 (2013) 1–7.
[36] M. Seifollahi Bazarjani, M. Hojamberdiev, K. Morita, et al., J. Am. Chem. Soc. 135 (2013) 4467–4475.
[37] J. Fu, Q. Xu, J. Low, C. Jiang, J. Yu, Appl. Catal. B 243 (2019) 556–565.
[38] Q. Zhai, S. Xie, W. Fan, et al., Angew. Chem. Int. Ed. 52 (2013) 5776.